PAPER

Systemic siRNA delivery to tumors by cell-penetrating α-helical polypeptide-based metastable nanoparticles†

Yang Liu,[a] Ziyuan Song, [ID] [a] Nan Zheng,[a] Kenya Nagasaka,[b] Lichen Yin [ID] *[c] and Jianjun Cheng [ID] *[a,c,d,e,f,g,h,i]

Systemic, non-viral siRNA delivery for cancer treatment is mainly achieved *via* condensation by cationic materials (*e.g.*, lipids and cationic polymers), which nevertheless, suffers from poor serum stability, non-specific tissue interaction, and unsatisfactory membrane activity against efficient *in vivo* gene knockdown. Here, we report the design of a metastable, cancer-targeting siRNA delivery system based on two functional polymers, PVBLG-8, a cationic, helical cell-penetrating polypeptide, and poly(L-glutamic acid) (PLG), an anionic random-coiled polypeptide. PVBLG-8 with rigid, linear structure showed weak siRNA condensation capability, and PLG with flexible chains was incorporated as a stabilizer which provided sufficient molecular entanglement with PVBLG-8 to encapsulate the siRNA within the polymeric network. The obtained PVBLG-8/siRNA/PLG nanoparticles (PSP NPs) with positive charges were sequentially coated with additional amount of PLG, which reversed the surface charge from positive to negative to yield the metastable PVBLG-8/siRNA/PLG@PLG (PSPP) NPs. The PSPP NPs featured desired serum stability during circulation to enhance tumor accumulation *via* the enhanced permeability and retention (EPR) effect. Upon acidification in the tumor extracellular microenvironment and intracellular endosomes, the partial protonation of PLG on PSPP NPs surface would lead to dissociation of PLG coating from NPs, exposure of the highly membrane-active PVBLG-8, and surface charge reversal from negative to positive, which subsequently promoted tumor penetration, selective cancer cell internalization, and efficient endo-lysosomal escape. When siRNA against epidermal growth factor receptor (EGFR) was encapsulated, the PSPP NPs showed excellent tumor penetration capability, tumor cell uptake level, EGFR silencing efficiency, and tumor growth inhibition efficacy in U-87 MG glioblastoma tumor spheroids *in vitro* and in xenograft tumor-bearing mice *in vivo*, outperforming the PSP NPs and several commercial reagents such as Lipofectamine 2000 and poly(L-lysine) (PLL). This study therefore demonstrates a facile and unique design approach of metastable and charge reversal NPs, which overcomes multiple biological barriers against systemic siRNA delivery toward anti-cancer treatment.

Introduction

RNA interference (RNAi) is a post-transcriptional regulation process mainly mediated by small interfering RNA (siRNA), which leads to mRNA degradation in a sequence-specific manner. RNAi has emerged as a promising therapeutic modality for cancer treatment.[1–9] Compared to chemotherapy with poor therapeutic selectivity and unsatisfactory

[a]Department of Materials Science and Engineering, University of Illinois at Urbana-Champaign, Illinois 61801, USA. E-mail: jianjunc@illinois.edu
[b]School of Molecular and Cellular Biology, University of Illinois at Urbana-Champaign, Illinois 61801, USA
[c]Jiangsu Key Laboratory for Carbon-Based Functional Materials & Devices, Institute of Functional Nano & Soft Materials (FUNSOM), Collaborative Innovation Center of Suzhou Nano Science and Technology, Joint International Research Laboratory of Carbon-Based Functional Materials and Devices, Soochow University, Suzhou 215123, China. E-mail: lcyin@suda.edu.cn
[d]Frederick Seitz Materials Research Laboratory, University of Illinois at Urbana-Champaign, Urbana, IL 61801, USA
[e]Department of Bioengineering, University of Illinois at Urbana-Champaign, Urbana, IL 61801, USA
[f]Beckman Institute for Advanced Science and Technology, University of Illinois at Urbana-Champaign, Urbana, IL 61801, USA
[g]Department of Chemistry, University of Illinois at Urbana-Champaign, Urbana, IL 61801, USA
[h]Carl R. Woese Institute for Genomic Biology, University of Illinois at Urbana-Champaign, Urbana, IL 61801, USA
[i]Micro and Nanotechnology Lab, University of Illinois at Urbana-Champaign, Urbana, IL 61801, USA
† Electronic supplementary information (ESI) available. See DOI: 10.1039/c8nr03976c

efficacy,[10,11] RNAi provides a more selective and specific treatment paradigm to regulate the abnormal genes in cancer cells.[12,13] Most of the current siRNA therapeutics in the clinical trials utilize direct administration into local target sites such as the eye and lung.[14] Due to the difficulty in locating the tumor areas or defining the margins of tumors such as glioma,[2,15] it is necessary to develop the systemically delivered siRNA formulation.

Cationic polymers, such as chitosan, poly(L-lysine) (PLL), and polyethylenimine (PEI), have been widely applied in siRNA delivery by forming stable, charged nanoparticles (NPs) via electrostatic complexation with siRNA.[16,17] While efficient in siRNA complexation, these carriers often lack strong membrane activities toward intracellular siRNA delivery, and endo-lysosomal entrapment post endocytosis always remains a critical hurdle against polycation-mediated siRNA delivery. Additionally, because siRNA is short and linear nucleic acid, polycations with high cationic charge density are often required to enable efficient complexation with siRNA and to promote the interaction with cell membranes toward potentiated gene silencing efficiency.[18] However, the positive surface charges could also interact with the negatively charged serum proteins during circulation, which provokes capture of NPs by the reticuloendothelial system (RES) tissues (such as liver and spleen) yet low distribution levels in tumors. PEGylation is the most commonly utilized approach to address this issue, which shields the surface positive charges to improve serum stability, prolong blood circulation, and facilitate passive tumor targeting.[19,20] Nevertheless, PEGylation at the meantime reduces the binding affinity between NPs and cell membranes, which prevents effective tumor accumulation and cell uptake to hinder the gene knockdown efficiency[21,22] Sheddable PEGylation that could be removed in response to tumor-specific triggers serves as an alternative strategy, which however, requires tedious chemical synthesis with difficulty in consistency control. Therefore, development of a serum-stable and cancer-targeting siRNA delivery system capable of potent and selective tumor penetration and membrane permeation is of great interest toward anti-cancer gene therapy.

Recently, we developed PVBLG-8, a unique membrane-penetrating, cationic polypeptide, which possesses stable α-helical secondary structure and helix-dependent membrane penetration capability with 1–2 orders of magnitude higher than conventional cationic polypeptides such as PLL or short cell penetrating peptides (CPPs) such as HIV-Tat and Arg9.[2,23–28] As a result, it can condense DNA and demonstrates potent DNA transfection efficiencies to outperform commercial transfection reagents such as Lipofectamine 2000. However, it shows poor siRNA complexation capability and only results in a loosely condensed structure, mainly because siRNA is linear and rod-like structure with few anionic charges compared to DNA molecules, which provides insufficient molecular entanglement or electrostatic interaction with PVBLG-8 that also adopts linear and rigid rod-like structure.[23]

To enhance the siRNA encapsulation efficiency of PVBLG-8, we were inspired by the success of PVBLG-8/DNA and other polycations/DNA encapsulation mechanisms, and herein incorporated poly(L-glutamic acid) (PLG), a biodegradable and biocompatible anionic polypeptide already used in multiple clinical trials,[29] for the formation of PVBLG-8/siRNA complexes.[30,31] Similar to DNA, PLG possesses rich negative charges and flexible backbone to allow efficient complexation with PVBLG-8 via molecular entanglement.[32] When PLG and siRNA were co-complexed with PVBLG-8, PLG serves as a physical crosslinker to promote and stabilize the formation of NPs, and in the meantime to facilitate effective encapsulation of siRNA into the polymeric nano-structure. PVBLG-8/siRNA/PLG (PSP) NPs with positively charged surfaces were thus obtained (Scheme 1). Similar to other polycationic siRNA delivery NPs, PSP NPs also suffer from poor serum stability, tumor accumulation, and non-specific membrane penetration.

The microenvironment of tumor offers various biomarkers to distinguish it from normal tissues.[33–35] In particular, the acidic pH in the extracellular compartment of tumor tissues has attracted great interest for the development of pH-responsive systems toward tumor-specific drug delivery.[36–40] By taking advantage of this unique tumor-specific physiology, NPs could be designed to be non-charged or negatively charged during systemic circulation while transform into positively charged state in response to the acidic pH to enable cancer-specific tumor penetration and cellular internalization.[19,41] In support of such strategy, the surface of PSP NPs was further coated with PLG, yielding the metastable PVBLG-8/siRNA/PLG@PLG (PSPP) NPs with negatively charged surfaces which accordingly afforded desired serum stability and enhanced tumor accumulation (Scheme 1). In the acidic extracellular compartment in the tumor tissues, the surface PLG could be partially protonated, thus triggering removal of the PLG coating and exposure of the cationic, membrane-active PVBLG-8 to subsequently potentiate the tumor penetration,
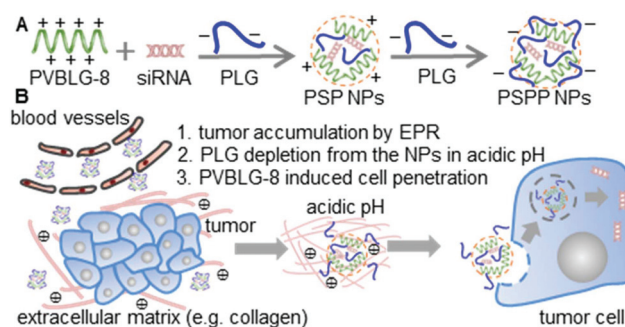
Scheme 1 Tumor-targeted siRNA delivery mediated by metastable NPs based on cell penetrating α-helical polypeptide, PVBLG-8. (A) PLG is incorporated during the formation of PVBLG-8/siRNA complexes to facilitate and stabilize the formation of positively charged PSP NPs. They were further coated with additional PLG to yield negatively charged PPSP NPs with increased serum stability and prolonged blood circulation. (B) After accumulation of the PPSP NPs in the tumor tissues through the EPR effect, the acidic extracellular pH triggers detachment of the PLG outer shell from the NPs surface, thus exposing the membrane-active PVBLG-8 to induce efficient cellular internalization of NPs.

cell internalization, and endosomal escape for efficient RNAi. Unlike previously reported charge-reversal strategy using acid-cleavable covalent conjugation with neutral or negative moieties, the metastable PLG coating offered an immediate and quick response to the acidic tumor microenvironment to enable de-shielding.[42] siRNA against endothelial growth factor receptor (EGFR), a growth factor receptor that induced cell differentiation and proliferation upon activation through the binding of its ligands and overexpressed in many types of tumors,[43] was encapsulated by the PSPP NPs. The tunable tumor penetration, cancer-selective cell internalization, EGFR knockdown efficiency, and anti-tumor efficacy were mechanistically explored in U-87 MG glioblastoma tumor spheroids *in vitro* and in xenograft tumor-bearing mice *in vivo*.

Experimental

Materials, cells, and animals

EGFR siRNA duplex and negative control siRNA with scrambled sequences (sc) were purchased from Integrated DNA Technologies (Coralville, Iowa, USA) and were dissolved in DEPC-treated water before use. The siRNA sequences were shown in Table S1.† Cy3-labeled EGFR siRNA duplex (Cy3-siRNA) was used for *in vitro* cell uptake studies, while Cy5-labeled EGFR siRNA duplex (Cy5-siRNA) was used for the *in vivo* imaging study. PVBLG-8 was synthesized following previously published procedures.[2]

U-87 MG cells (human glioblastoma) were purchased from the American Type Culture Collection (Rockville, MD, USA), and were cultured in DMEM supplemented with 10% fetal bovine serum (FBS). HEK-293 cells were kindly provided by Prof. Kemper (University of Illinois at Urbana-Champaign) and were cultured in DMEM containing 10% FBS.

Athymic nude mice (8–10 weeks) were obtained from Charles River Laboratory (Wilmington, MA, USA) and were housed in an SPF room with four mice per cage. Mice were given access to water *ad libitum* and exposed to a 12 : 12 h light–dark cycle (7 : 00 am–7 : 00 pm) at 25 ± 1 °C. All animal studies were performed in strict accordance with the NIH guidelines for the care and use of laboratory animals (NIH Publication No. 85–23 Rev. 1985). The animal experimental protocols were approved by the Institutional Animal Care and Use Committees (IACUC) of University of Illinois at Urbana-Champaign.

Instrumentation

^{1}H NMR spectra were recorded on a Varian U500 (500 MHz) spectrometer. Electrospray ionization mass spectrometry (ESI-MS) was performed on a Waters Quattro-Mass Spectrometer. Matrix Assisted Laser Desorption Ionization-Time Of Flight mass spectrometry (MALDI-TOF-MS) was performed on an Applied Biosystems Voyager-DE STR Time of Flight instrument or a Bruker Daltonics UltrafleXtreme MALDI-TOF instrument in positive-ion mode with 2,5-dihydroxybenzoic acid as a matrix. Gel permeation chromatography

(GPC) experiments were performed on a system equipped with an isocratic pump (Model 1100, Agilent Technology, Santa Clara, CA, USA), a DAWN HELEOS multi-angle laser light scattering (MALLS) detector (Wyatt Technology, Santa Barbara, CA, USA), and an Optilab rEX refractive index detector (Wyatt Technology, Santa Barbara, CA, USA). The detection wavelength of HELEOS was set at 658 nm. Separations were performed using serially connected size exclusion columns (100 Å, 500 Å, 10³ Å, and 10⁴ Å Phenogel columns, 5 μm, 300 × 7.8 mm, Phenomenex, Torrance, CA, USA) at 60 °C using DMF containing 0.1 M LiBr as the mobile phase. The MALLS detector was calibrated using pure toluene with no need for calibration using polymer standards and can be used for the determination of the absolute molecular weights (MWs). The MWs of polymers were determined based on the dn/dc value of each polymer sample calculated offline using the internal calibration system processed by the ASTRA V software (Version 5.1.7.3, WyattTechnology, CA, USA). Lyophilization was performed on a FreeZone lyophilizer (Labconco, MO, USA).

Preparation and characterization of NPs

PVBLG-8 and PLG were synthesized as previously reported[26] with polymerization degrees of 195 and 50, respectively. siRNA, PVBLG-8, and PLG were separately dissolved in DEPC-treated water at 0.2, 1, and 1 mg mL^{-1}, respectively. siRNA and PLG were mixed (1 : 5, w/w), into which PVBLG-8 was added at the PVBLG-8/PLG weight ratio of 10 : 1. The mixture was vortexed for 30 s and incubated at 37 °C for 30 min to obtain the PSP NPs. The PSP NPs were further coated with PLG *via* addition of the PLG solution (1 mg mL^{-1} in DEPC water) at various PLG/PVBLG-8 weight ratios with gentle shaking, thus achieving the PLG-coated PSP (PPSP) NPs. A gel retardation assay was used to evaluate the siRNA condensation efficiency. Briefly, NPs or naked siRNA were loaded in 4% agarose gel followed by electrophoresis at 56 V for 1 h and visualization of siRNA migration using the gel documentation. The NPs were also subjected to size and zeta potential measurement using dynamic light scattering (DLS, Zetasizer Nano-ZS, Malvern Instruments, UK). To explore the detachment of surface PLG from NPs, the zeta potentials of NPs were monitored at different pH values (7.4, 6.5, and 5.5). To evaluate the stability of NPs in serum, NPs were diluted with DMEM containing 10% FBS for 10 fold and incubated at RT for 2 h before size measurement using DLS.

Stability of siRNA in NPs

In order to evaluate the *in vivo* stability of siRNA following systemic administration, siRNA-containing NPs or naked siRNA were incubated with 10% mouse serum at 37 °C for 2 h. The mixture was heated at 80 °C for 5 min to deactivate the nucleases, and heparin (1000 U mL^{-1}) was then added to dissociate the siRNA. The mixture was loaded on 4% agarose gel followed by electrophoresis at 56 V for 1 h, and the siRNA integrity was visualized by gel documentation.

Cellular uptake

U-87 MG cells were seeded on 24-well plates at 5×10^4 cells per well and cultured for 24 h. To mimic the acidic pH in the tumor environment, the medium was replaced by HBSS (pH 6.5), and Cy3-siRNA-containing NPs or naked Cy3-siRNA were added (0.4 μg siRNA per well, 200 μL per well) followed by incubation at 37 °C for 4 h. Poly(ʟ-lysine) (PLL, MW = 70–150 kDa)/siRNA NPs (w/w = 20 : 1) were incorporated as a control. Cells were washed with PBS for three times and then lysed with the RIPA lysis buffer (100 μL). The Cy3-siRNA level in the lysate was determined by spectrofluorimetry (λ_{ex} = 480 nm, λ_{em} = 520 nm), and the total protein content was determined using the BCA kit. The cell uptake level was expressed as the fluorescence intensity of Cy3-siRNA per 1 mg of cellular protein.

To explore the endosomal escape of NPs, cells were co-incubated with Lysotracker Green and Cy3-siRNA-containing NP at pH 6.5 for 0.5 h and 2 h at 37 °C, respectively. Cells were than fixed with 4% paraformaldehyde (PFA), nuclei-stained with Hoechst, and observed by CLSM (Confocal laser scanning microscopy) (Model 700, Zeiss, Germany).

HEK293 cells were incubated with naked siRNA, PSP NPs and PSPP NPs in HBSS (pH 7.4) for 4 h, respectively. Cells were washed with PBS three times and then lysed with the RIPA lysis buffer. The fluorescence intensity of Cy3-siRNA in the lysate was determined by spectrofluorimetry (λ_{ex} = 480 nm, λ_{em} = 520 nm); the total protein content was determined by BCA assay. Uptake level was expressed as the fluorescence intensity of Cy3-siRNA per mg of cellular protein.

In vitro penetration in 3D tumor spheroids

Low-melting-point agarose was dissolved in sterile PBS (pH 7.4) at the final concentration of 1.5%.[44] The agarose solution was added to 96-well plate (50 μl per well), and agarose-coated plates were obtained after being fully cooled. The agarose-coated plates were exposed under UV light for 30 min for sterilization. U-87 MG cells were then seeded on the agarose-coated plates at 1×10^5 cells per well and cultured for 7 days to allow formation of 3D tumor spheroids. The medium was changed every other day. PPSP NPs prepared from Alexa Fluor-488-labeled PLG and Cy3-siRNA were added (0.4 μg siRNA per well, 200 μL per well) and incubated with spheroids in serum-free medium (pH 6.5 or 7.4) for 4 h. Then, the tumor spheroids were washed with PBS for three times and fixed with 4% PFA. Cell nuclei were stained with Hoechst, and the penetration of NPs into tumor spheroids was observed by CLSM (Model 700, Zeiss, Germany).

In vitro EGFR knockdown in U-87 MG cells

U-87 MG cells were seeded on 6-well plates at 5×10^5 cells per well and cultured for 24 h. The medium was changed to serum-free DMEM (pH 6.5), and PPSP NPs were added at pre-determined siRNA concentrations. Following incubation for 4 h, the medium was replaced with serum-containing DMEM, and cells were further cultured for 20 h. The EGFR mRNA level

was determined by real-time PCR, and results were represented as the percentage of EGFR mRNA levels of control cells that did not receive NPs treatment. To prepare the samples for real-time PCR analysis, RNA was isolated from cells using the QIAGEN RNeasy Mini Kit. cDNA was synthesized from 5 μg of total RNA using high capacity cDNA reverse transcription kit (Applied Biosystems, CA, USA) according to the manufacturer's protocol. Synthesized cDNA, EGFR primers (forward and reverse, sequences shown in Table S2†), and SYBR Premix Ex Taq™ were mixed and run on an ABI PRISM 7900HT Real-Time PCR system (Applied Biosystems, CA, USA). The GAPDH mRNA was used as an internal loading control, and its expression did not change upon addition of NPs or siRNA.

In vitro anti-tumor efficacy in 3D tumor spheroids

The 3D tumor spheroids were prepared as described above. On day 3 post tumor cell seeding, the spheroids were treated with different NPs in HBSS (pH 6.5 or 7.4) for 4 h. The spheroids were further cultured for 20 h, and the EGFR mRNA levels in the tumor spheroids were determined by real-time PCR. Sizes of the spheroids treated by various NPs at pH 6.5 were observed by optical microscopy on day 3, 6 and 9 post tumor cell seeding, and the length and width of the tumor spheroids were determined. The spheroid volume was calculated as: $V = 1/2 \times L \times W \times W$ (L and W being the length and width of the tumor spheroids, respectively). Five tumor spheroids were calculated for each tested group.

In vivo biodistribution

U-87 MG cells were suspended in PBS (50 μL, 2×10^6 cells), mixed with 25 μL of Matrigel (BASEMENT MEMBRANE MATRIX, BD Medical Technology, USA), and injected subcutaneously into nude mice on the right flank. When the tumor volume reached 100 mm³ (usually within 10 days), PSP NPs or PPSP NPs containing Cy5-siRNA were intravenously (i.v.) injected (1 mg siRNA per kg, 200 μL). At 1 and 4 h post injection, animals were anesthetized with 3% isoflurane and imaged by a Maestro *In Vivo* Imaging System (PerkinElmer, MA, USA) using green excitation filter (572–621 nm) with the exposure time of 100 ms. Mice were then euthanized, and the tumors as well as major organs (heart, liver, spleen, lung, and kidney) were harvested before being imaged using the Maestro *In Vivo* Imaging System as well. The tumor tissues were further frozen in the OCT embedding medium (Sakura, CA, USA). Frozen sections of 20 μm thickness were prepared with a cryotome Cryostat (CM 1900, Leica, Germany), and were stained with Hoechst (300 nM) for 15 min at room temperature. After washing with PBS for twice, the frozen sections were mounted with the Prolong Gold® (Invitrogen) mounting medium and observed under CLSM (Model 700, Zeiss, Germany).

In vivo anti-cancer efficacy

U-87 MG tumor-bearing mice were prepared as described above. When the tumor volume reached 100 mm³, PSP NPs or PPSP NPs were i.v. injected at 1 mg siRNA per kg every three days for a total of three injections (6 mice in each group). PLL/

siRNA NPs or saline served as controls. The tumor size and body weight were monitored every 3 days within the observation period of 15 days. The tumor size was calculated as $V = 1/2 \times L \times W \times W$ (L and W being the length and width of the tumor, respectively).

In vivo EGFR knockdown

Tumors were harvested on day 15 post the first injection of NPs as described above (6 mice in each group). RNA was isolated from tumors using the QIAGEN RNeasy Mini Kit, and the EGFR mRNA level was determined by real-time PCR using the same method as mentioned above. Results were denoted as the percentage of EGFR mRNA levels of the control mice that did not receive NPs treatment.

The EGFR expression level was further explored by immunostaining. The tumors were fixed with 4% PFA, frozen in OCT, and cryo-sectioned to obtained 20 μm thick sections. They were incubated with Anti-EGFR antibody (Santa Cruz Biotechnology, CA, USA) at 4 °C overnight. After washing with PBS for three times, the tumor sections were incubated with Alexa Fluor-555 labeled secondary antibody for another 2 h. Then, the sections were stained with Hoechst (300 nM) for 15 min at room temperature. After washing twice with PBS, the sections were mounted with Prolong Gold® (Invitrogen) and observed by CLSM (Model 700, Zeiss, Germany).

Results and discussion

Characterization, siRNA encapsulation, and stability of PSPP NPs

PVBLG-8 possesses α-helical secondary structure, which is more rigid than other typical cationic polymers that adopt flexible, random-coil structure. Although PVBLG-8 can condense plasmid DNA to form stable NPs through electrostatic interaction,[23,28] it only forms loosely packed complexes upon mixing with siRNA, presumably due to the rigid structure of both molecules and the low molecular weight of siRNA that prohibit efficient complexation with PVBLG-8. The resulting loosely packed complexes showed relatively large particle size of ∼500 nm and high polydispersity index (PDI) of 0.213, along with low siRNA encapsulation efficiency of <20% at the PVBLG-8/siRNA weight ratio up to 20 (Fig. 1A). To address this issue, PLG, a random-coiled polyanion, was incorporated as a stabilizer to facilitate the complexation between positively charged PVBLG-8 and negatively charged siRNA and PLG, wherein PLG provided sufficient molecular entanglement with PVBLG-8 to encapsulate the siRNA within the polymeric network. PVBLG-8 was firstly complexed with PLG at different ratios as shown in Table S3.† The optimal PVBLG-8/PLG weight ratio of 10 was identified and used in further studies, because of the relatively small particle size (∼88 nm) and positive surface charge (∼10 mV) of the PSP NPs at this ratio (Fig. S1A and B†). In attempts to convert the surface charge of NPs from positive to negative, additional PLG was coated onto the PSP NPs, yielding the negatively charged PSPP NPs. As
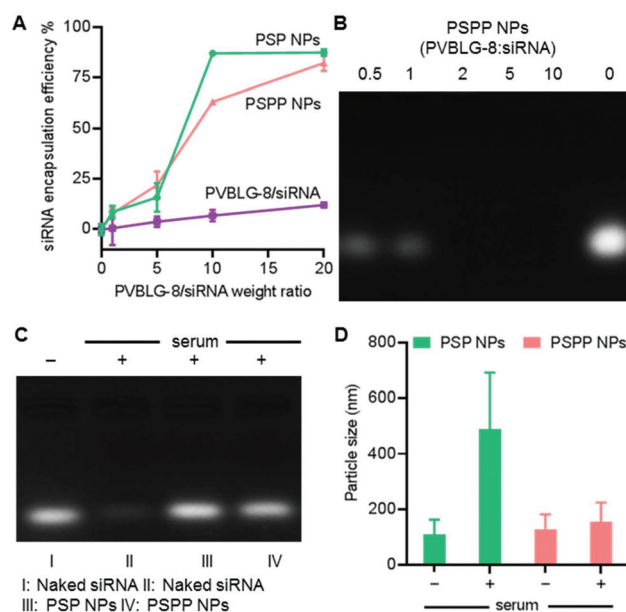

Fig. 1 Characterization of NPs. (A) siRNA encapsulation efficiencies in PS, PSP, and PPSP NPs as determined by the EB exclusive assay. (B) Gel retardation assay showing siRNA migration in 4% agarose gel. PSPP NPs with various PVBLG-8/siRNA weight ratios were utilized (PVBLG-8/PLG = 10 : 1.5, w/w). (C) Gel retardation assay for stability of naked siRNA or siRNA loaded in NPs following treatment with mouse serum for 2 h. (D) Size alteration of PSP and PPSP NPs upon incubation with 10% mouse serum for 2 h.

expected, zeta potential of the NPs decreased with increased amount of coated PLG, and PSPP NPs with negative zeta potential were obtained at the PLG (coating)/PVBLG-8 weight ratios ≥0.15 (Fig. S1B†). Particle size slightly increased upon coating with additional PLG (Fig. S1A†). The optimal PLG (coating)/PVBLG-8 weight ratio of 0.15 was identified, because of the smallest diameter and negative zeta potential of the PSPP NPs at such ratio (PVBLG-8/siRNA/PLG (complexing)/PLG (coating) = 10/0.5/1/1.5, w/w/w/w). The siRNA encapsulation efficiency was further evaluated using the EB exclusion assay and gel retardation assay. In comparison to PVBLG-8/siRNA NPs that afforded siRNA encapsulation efficiency of only ∼10% at high weight ratio of 20, both PSP and PSPP NPs showed notably enhanced siRNA encapsulation efficiencies of >80% at the PVBLG-8/siRNA weight ratio of 20 with fixed PVBLG-8/PLG weight ratio (Fig. 1A). Similarly, the PSPP NPs were able to completely retard the migration of siRNA upon agarose gel electrophoresis at the PVBLG-8/siRNA weight ratio ≥2 (Fig. 1B), wherein PVBLG-8 alone could not retard the siRNA migration at the high PVBLG-8/siRNA weight ratio up to 20 as reported in our previous research.[23] Because of the efficient encapsulation of siRNA into the nanostructure, stability of siRNA against serum was greatly enhanced as evidenced by the clear siRNA band after gel electrophoresis (Fig. 1C). Comparatively, free siRNA was largely degraded after serum treatment for 2 h. After incubation with serum, the particle size of the positively charged PSP NPs dramatically increased, while that of the

negatively charged PSPP NPs only slightly changed (Fig. 1D). It thus demonstrated that surface coating of PSP NPs with additional PLG greatly enhanced the serum stability of the NPs by shielding the positive surface charges, which would further benefit prolonged blood circulation and tumor accumulation.[45]

In vitro cellular uptake of PSPP NPs

We next studied the cellular uptake of PSPP NPs in U-87 MG glioblastoma cells at pH 6.5 (Fig. 2A). Compared with the positively charged PLL/siRNA NPs, cellular uptake level of the PSPP NPs was 2.7 fold higher, presumably due to the high membrane activity of the exposed helical PVBLG-8 from PSPP NPs at lowered pH in subcellular compartment that was capable of pore formation to facilitate effective transmembrane delivery of gene cargoes.[46] To explore the selectivity in terms of cellular internalization, HEK-293 cells (normal cell line) were incubated with the PSPP NPs or PSP NPs at pH 7.4 and in the presence or absence of serum. Due to their positively charged nature, PSP NPs showed appreciable cell uptake level in the absence of serum, indicating lack of selectivity between normal and cancerous cells (Fig. S2†). The cell uptake level

was dramatically diminished in the presence of serum, mainly because of the low stability of the positively charged NPs in serum that led to particle aggregation/dissociation. In comparison, PSPP NPs showed minimal cellular uptake level both in the presence and absence of serum at pH 7.4, because the surface coating of PLG shielded the cationic charges to prevent non-specific cellular internalization in normal cells at neutral pH. Such findings therefore demonstrated that PSPP NPs were capable of mediating selective and potent internalization into cancer cells due to de-shielding of the PLG coating at acidic pH in the tumor extracellular compartment followed by the helical PVBLG-8-mediated potent membrane penetration.

The successful delivery of siRNA into the cytoplasm of U-87 MG cells mediated by PSPP NPs at pH 6.5 was also confirmed by CLSM (Fig. 2B). Extensive red fluorescence (Cy3-siRNA) was noted in the cytoplasm, and it largely separated from the green fluorescence (Alexa Fluor 488-labeled PLG), indicating that PSPP NPs efficiently delivered siRNA into U-87 MG cells and siRNA could be released in the cytoplasm after cellular internalization.

To further study the endosomal escape of siRNA, a critical step toward effective gene transfection, the endosome was
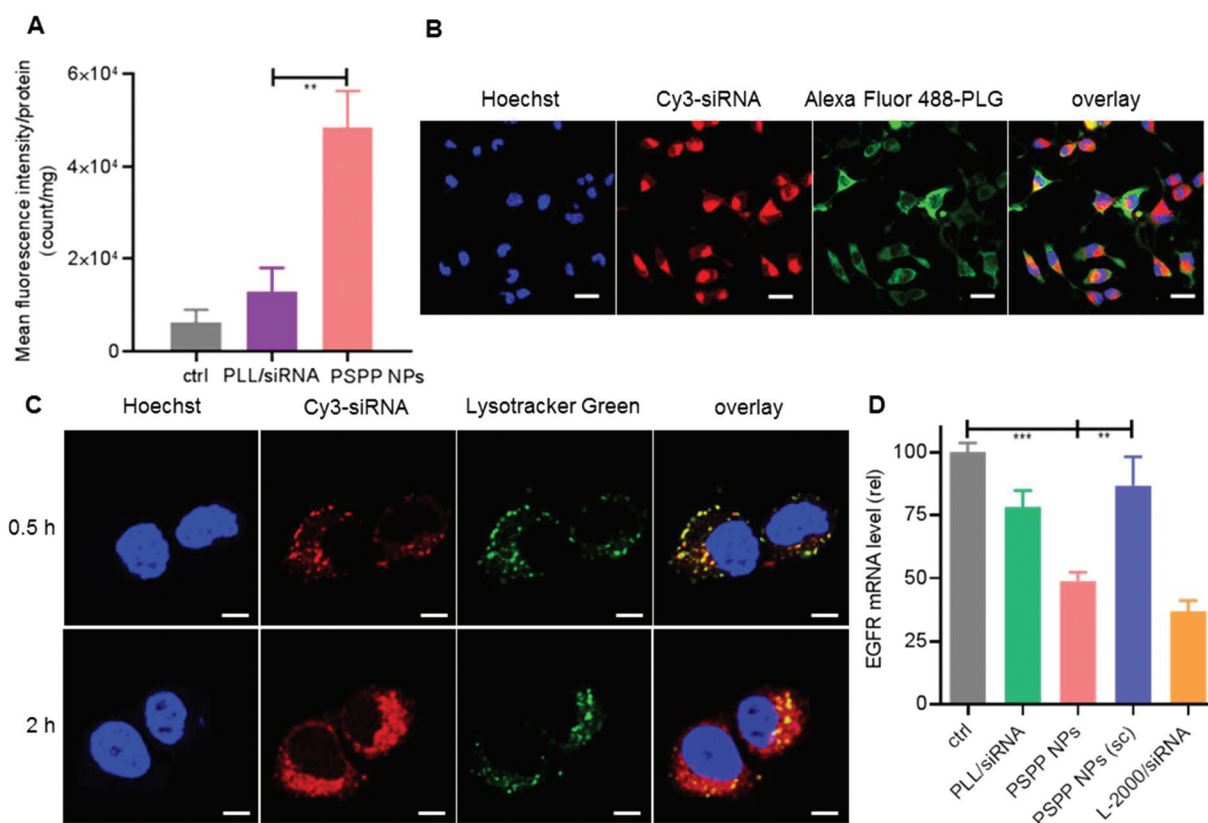

Fig. 2 *In vitro* cell uptake of NPs and EGFR knockdown in U-87 MG cells. (A) Cellular uptake level of Cy3-siRNA-loaded NPs at pH 6.5 ($n = 4$, *$p < 0.05$; **$p < 0.005$; ***$p < 0.001$). (B) CLSM images of U-87 MG cells after treatment with PSPP NPs containing Cy3-siRNA (red) and Alexa Fluor 488-PLG (green) for 4 h at pH 6.5. Cell nuclei were stained with Hoechst (blue). Bar represents 5 μm. (C) CLSM images U-87 MG cells following treatment with PSPP NPs loaded with Cy3-siRNA (red) at pH 6.5 for 0.5 or 2 h. Cell nuclei were stained with Hoechst (blue), and *endo*-lysosomes were stained with Lysotracker Green (green). Bar represents 5 μm. (D) Relative EGFR mRNA level in U-87 MG cells after treatment with various NPs at pH 6.5 ($n = 4$, *$p < 0.05$; **$p < 0.005$; ***$p < 0.001$).

stained with Lysotracker Green and its colocalization with Cy3-siRNA was observed by CLSM. As shown in Fig. 2C, after 0.5 h incubation of cells with Cy3-siRNA-containing PSPP NPs, Cy3-siRNA signal mainly co-localized with Lysotracker-stained endosomes, suggesting that the PSPP NPs was internalized mainly through endocytosis. Interestingly, after 2 h incubation, most of the Cy3-siRNA was found to spread out to the whole cytoplasm, indicating the efficient endosomal escape of

PSPP NPs mainly mediated by the membrane disruption property of the helical PVBLG-8.

In vitro EGFR silencing in U-87 MG cells

The gene silencing efficiency of PSPP NPs against EGFR expression at pH 6.5 was evaluated in U-87 MG cells by real-time PCR (Fig. 2D). The PSPP NPs led to 50% down-regulation of the targeted EGFR mRNA level, which was comparable to knockdown efficiency of Lipofectamine 2000 (~60%). However, the PLL/siRNA NPs as a control only resulted in 23% down-regulation of the EGFR mRNA level.

Penetration of PSPP NPs in U-87 MG tumor spheroids

The 3-D tumor spheroid was used to mimic the tumor tissues for the evaluation of tumor penetration.[47] PSPP NPs prepared from Alexa Fluor 488-labeled PLG (green fluorescence) and Cy3-siRNA (red fluorescence) were incubated with the tumor spheroids at pH 7.4 or 6.5, which simulates the neutral condition during circulation and the acidic condition in the tumor extracellular environment, respectively.
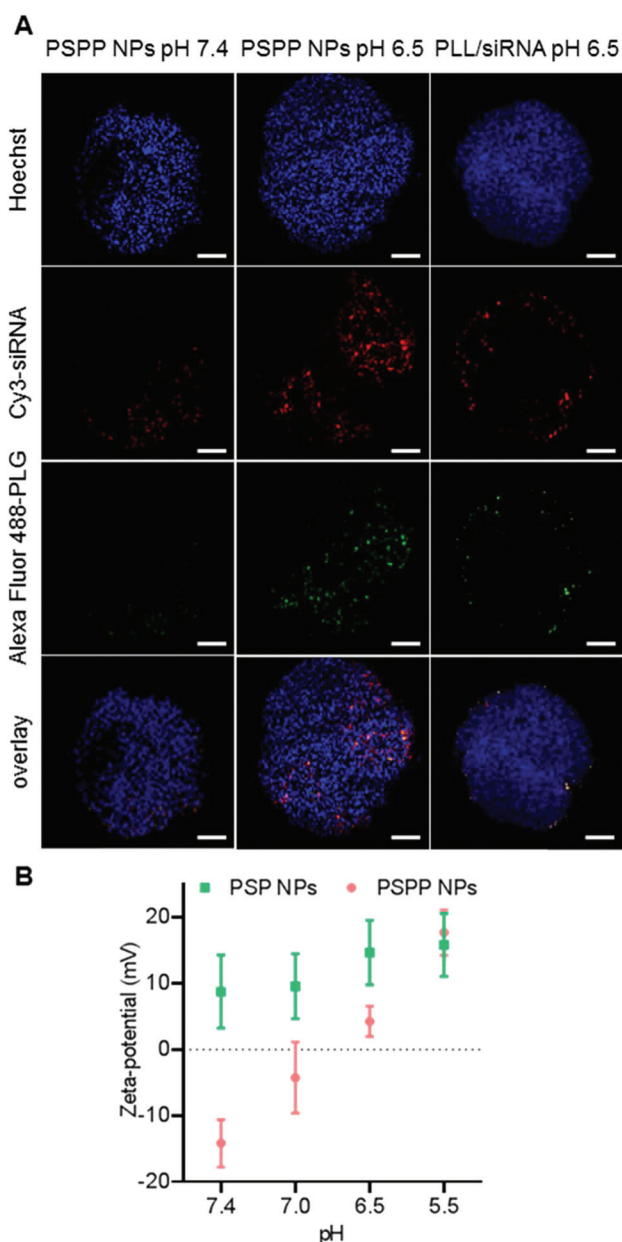

Fig. 3 (A) Acid-mediated de-shielding of PLG surface layers on PSPP NPs promotes tumor penetration of PPSP NPs. (A) CLSM images of U-87 MG tumor spheroids following treatment with Cy3-siRNA-containing PPSP NPs at pH 7.4 or 6.5 for 4 h. PLL/siRNA NPs were incorporated as a control. Scale bar represents 250 μm. (B) Zeta potentials of PSP NPs and PPSP NPs at different pH.
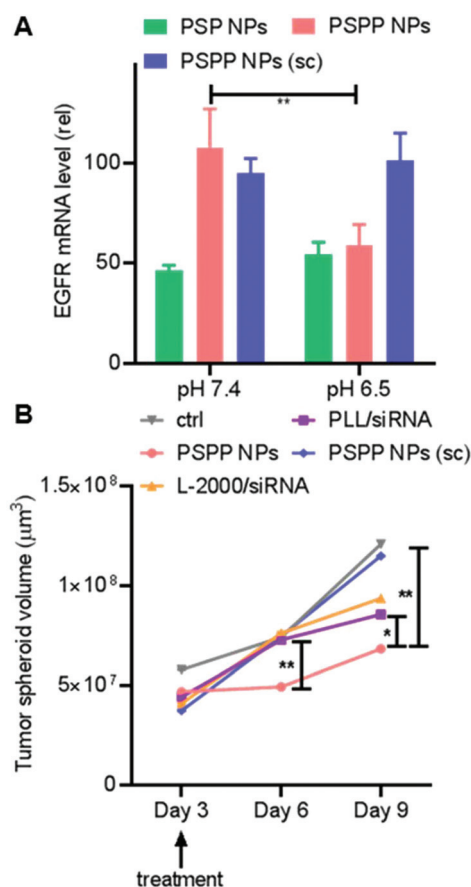

Fig. 4 EGFR silencing and anti-tumor efficacy of PSPP NPs in U-87 MG tumor spheroids. (A) EGFR mRNA levels in tumor spheroids after treatment with various NPs at pH 7.4 or 6.5 ($n = 3$, *$p < 0.05$; **$p < 0.01$; ***$p < 0.001$). (B) Volume changes of tumor spheroids within 6 days following treatment with various NPs at pH 6.5 ($n = 5$, *$p < 0.05$; **$p < 0.005$; ***$p < 0.001$).

Increased accumulation and deeper penetration of the PSPP NPs in tumor spheroids were observed at pH 6.5 compared with those at pH 7.4 (Fig. 3A). Cationic NPs normally exhibit higher tumor penetration capabilities than anionic NPs,[48] and thus the above different tumor accumulation/penetration properties of PSPP NPs at different pH could be attributed to the de-shielding of the PLG outer layer on the NPs surface that leads to the exposure of the cationic PVBLG-8 to promote the tumor accumulation. PLL/siRNA NPs as a control showed poor tumor penetration capability, and the Cy3-siRNA/Alexa Fluor 488-PLG fluorescence was mainly localized on the periphery of the spheroids. Similar results were obtained when the fluorescence distribution was further analyzed by Image J, revealing the deep penetration of PSPP NPs into tumor spheroids compared to the peripheral distribution of PLL/siRNA NPs (Fig. S3†). To further explore the acid-triggered de-shielding of surface PLG layers, the zeta potentials of PSPP NPs at different pH values from 7.4 to 5.5 were monitored in collagen-coated tubes. As the pH decreased, the zeta potential of the NP increased and reversed from negative to positive when pH reached 6.5 (Fig. 3B). It therefore verified the deprotonation of the outer PLG layer and its depletion from the surface of PSPP NPs, which accordingly allowed the exposure of PVBLG-8 because PLG was just loosely attached to the surface of PSP NPs in a metastable state.

In vitro gene silencing efficiency and anti-tumor efficacy of PSPP NPs in U-87 MG tumor spheroids

The extracellular environment of 3-D tumor spheroids was considered to be closer to that in the *in vivo* settings. Therefore, the gene silencing efficiency of PSPP NPs against EGFR expression in tumor spheroids was further determined by real-time PCR (Fig. 4A). The PSPP NPs led to 40% down-regulation of the EGFR mRNA level in tumor spheroids at pH 6.5, while in comparison, they showed negligible gene silencing at pH 7.4. On the other hand, the positively charged PSP NPs showed comparable gene silencing effects at pH 7.4 and pH 6.5 in tumor spheroids. Such discrepancy thus further substantiated that de-shielding of the PLG surface layer on PSPP NPs at acidic pH could enable the selective delivery into tumor cells to mediate EGFR gene silencing. PSPP NPs encapsulated with scrambled (sc) siRNA had no inhibitory effects on the EGFR mRNA level at either pH 6.5 or pH 7.4.

Growth of the tumor spheroid after treatment with different NPs at pH 6.5 was further monitored to evaluate the *in vitro* anti-cancer efficacy. The treatment began on the 3rd day of tumor spheroid seeding (Day 3). After 3 days post-treatment (Day 6), size of the tumor spheroid treated with PSPP NPs only increased by 6% compared with that of Day 3 (Fig. 4B), while the spheroids treated with PLL/siRNA NPs or Lipofectamine 2000/siRNA NPs increased by ∼50%. On day 9, even obvious
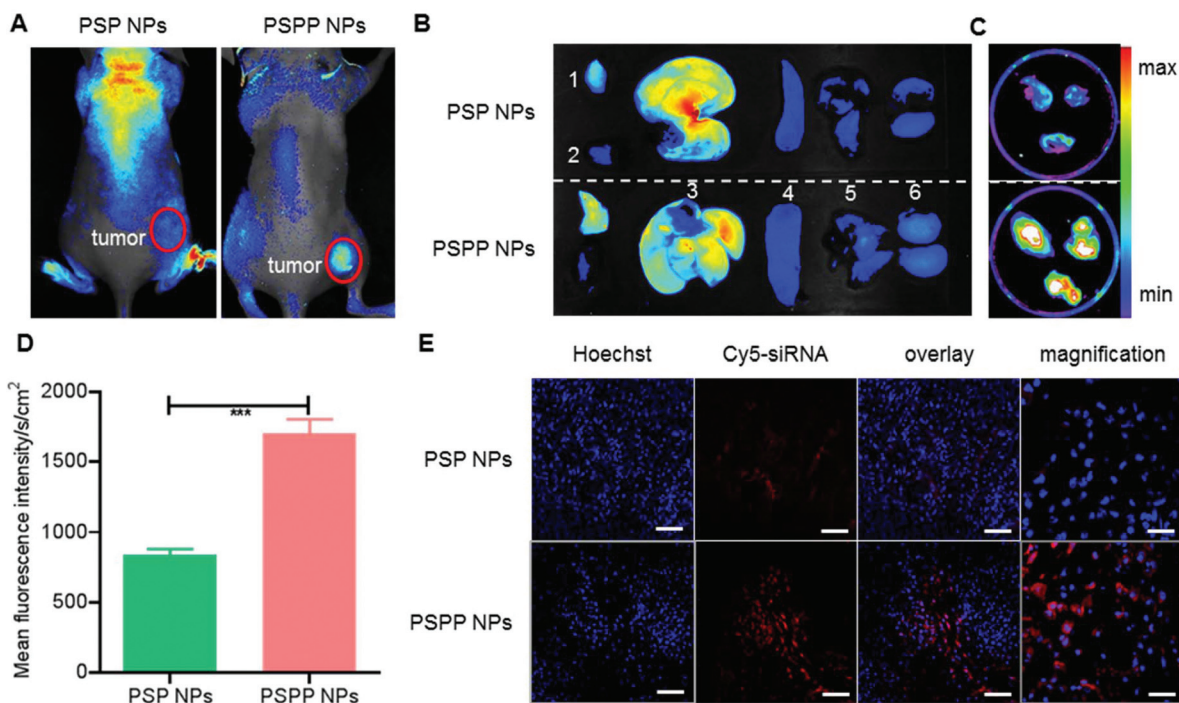

Fig. 5 Biodistribution of Cy5-siRNA-containing PSP or PPSP NPs in U-87 MG tumor-bearing mice at 4 h post i.v. injection (1 mg siRNA per kg). (A) Fluorescence imaging of whole animals. (B) Representative *ex vivo* imaging of tumors and major organs. 1. Tumor, 2. heart, 3. liver, 4. spleen, 5. lung, and 6. kidney. (C) *Ex vivo* imaging of tumors harvested from mice administered with PSP NPs (top) and PSPP NPs (bottom) (*n* = 3). (D) Calculated fluorescence intensities of Cy5-siRNA in *ex vivo* tumors in (C) (*n* = 3, *p < 0.05; **p < 0.005; ***p < 0.001). (E) CLSM images of tumor sections. Nuclei were stained with Hoechst. Scale bars represent 10 μm in column 1–3 and 2 μm in column 4.

disparity was noted wherein spheroid volume after treatment with PSPP NPs was only increased by 32%, while after treatment with PLL/siRNA NPs and Lipofectamine 2000/siRNA NPs, it was augmented by 84% and 102%, respectively. Such results further indicated the potent efficiency of PSPP NPs in tumor growth inhibition over PLL/siRNA NPs and Lipofectamine 2000/siRNA NPs.

In vivo biodistribution and tumor accumulation of PSPP NPs

The positively charged PSP NPs and negatively charged PSPP NPs were i.v. injected and the whole animal fluorescence imaging was performed at 4 h post injection (Fig. 5A). Animals receiving PSPP NPs showed notably stronger fluorescence signals in the tumor regions than those treated with PSP NPs. Similar results were observed when the tumor tissues were harvested and imaged, wherein the fluorescence intensity in PSPP NPs-treated tumors was comparable to that in PSPP NPs-treated liver tissues while notably higher than that in PSP NPs-

treated tumors (Fig. 5B–E). Such disparity was mainly because the negatively charged PSPP NPs could prevent the adsorption of serum proteins and thus prolong the blood circulation time and passive cancer targeting. CLSM observation of tumor sections also showed higher distribution level of Cy3-siRNA in PSPP NPs-treated tumors than in PSP NP-treated tumors (Fig. 5E), and the signals were mainly concentrated in the intracellular areas, indicating that PSPP NPs could be distributed to the tumor in a more effective way, and PVBLG-8 could mediate effective cell-penetration and endosomal escape after entering the tumor cells.

In vivo anti-tumor efficacy

Nude mice bearing U-87 MG xenograft tumors were i.v. injected with different NPs as well as saline. The treatment began when the tumor volume reached 100 mm^3 as the EPR effect was considered to be prevalent at this stage.[49,50] The body weights did not change significantly after administration
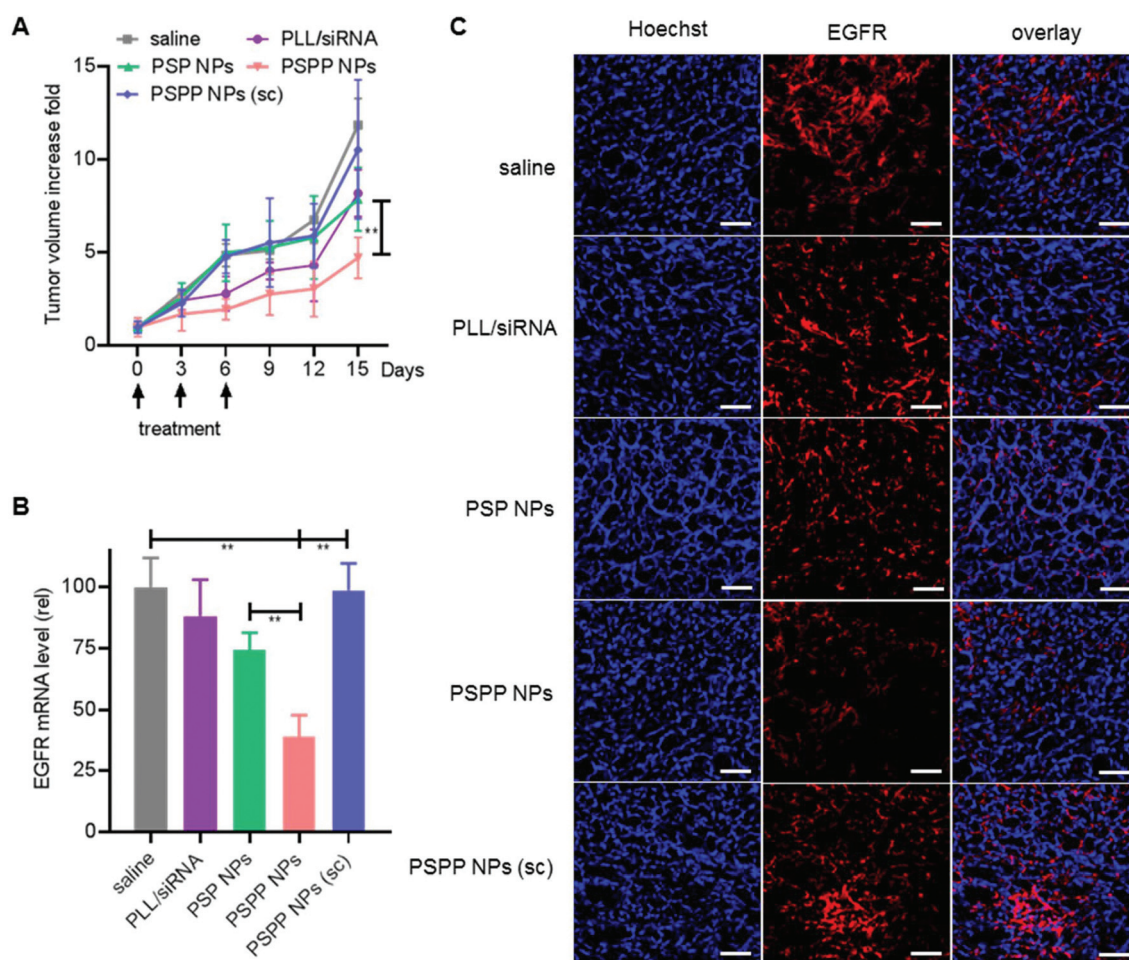

Fig. 6 EGFR knockdown efficiency and anti-tumor efficacy of i.v. injected NPs (1 mg siRNA per kg) in U-87 MG xenograft tumor-bearing mice. (A) Tumor volume changes over the observation period of 15 days ($n = 6$, *$p < 0.05$; **$p < 0.005$; ***$p < 0.001$). (B) Relative EGFR mRNA levels in tumors on Day 15 post the first NPs injection ($n = 6$, *$p < 0.05$; **$p < 0.005$; ***$p < 0.001$). (C) EGFR immunostaining of tumor sections harvested on Day 15 post the first NPs injection. Cell nuclei were stained with Hoechst. Scale bar represents 10 μm.

of different NPs, indicating their unappreciable toxicity (Fig. S4†). Tumor growth was notably inhibited after treatment with PSPP NPs containing EGFR siRNA, and it significantly outperformed the PLL/siRNA NPs and PSP NPs in terms of the anti-tumor efficacy (Fig. 6A). Consistently, PSPP NPs mediated significantly higher EGFR silencing efficiency than PLL/siRNA NPs and PSP NPs in tumor tissues, as evidenced by both real-time PCR (Fig. 6B) and EGFR immunostaining (Fig. 6C). The quantitative immunostaining staining analysis was shown in Fig. S5.† Such results accorded well with the *in vitro* results to substantiate the collective contribution of PLG-promoted tumor accumulation and PVBLG-8-mediated membrane penetration toward efficient EGFR siRNA delivery and anti-tumor treatment.

Conclusions

In summary, metastable NPs capable of tumor targeting, tumor penetration, and selective tumor cell internalization were developed based on membrane penetrating, helical polypeptide PVBLG-8 and anionic PLG, for the efficient encapsulation and delivery of EGFR siRNA. The rigid, linear structure of PVBLG-8 suffered from poor siRNA condensation capability, and PLG with linear and flexible chains was incorporated as a stabilizer to enhance the molecular entanglement with PVBLG-8 to remarkably strength the siRNA encapsulation. The obtained PSP NPs with positive surface charges were further coated with PLG to reverse the surface charge from positive to negative, and thus the obtained PSPP NPs featured desired serum stability during circulation to enhance tumor accumulation *via* the EPR effect. After accumulation of the PSPP NPs in the tumor tissues, the acidic extracellular condition (pH 6.5) triggered de-shielding of the PLG coating to expose the cationic, membrane-penetrating PVBLG-8, thus facilitating tumor penetration, cancer cell uptake, and endosomal escape of the NPs. Unlike the tumor cell endocytosis enhanced by ligand–receptor interaction, PVBLG-8-mediated intracellular delivery showed a receptor-independent pathway which was more efficient and universal that could also be applied in other tumor types. As a result, the PSPP NPs efficiently silenced the EGFR expression in U-87 MG tumor spheroids *in vitro* and tumor tissues *in vivo*, and notably inhibited the growth of tumor spheroids *in vitro* and xenograft tumors *in vivo*, outperforming the PSP NPs and commercial reagents such as Lipofectamine 2000 and PLL. Considering that acidic extracellular condition is a common microenvironment characteristic shared by most tumors, the PSPP NPs developed in this study can be further explored as a universal siRNA delivery nanoplatform for targeted and efficient cancer gene therapy.

Conflicts of interest

There are no conflicts to declare.

Acknowledgements

References

1 R. Kanasty, J. R. Dorkin, A. Vegas and D. Anderson, *Nat. Mater.*, 2013, **12**, 967–977.
2 N. P. Gabrielson, H. Lu, L. Yin, D. Li, F. Wang and J. Cheng, *Angew. Chem., Int. Ed.*, 2012, **51**, 1143–1147.
3 H. M. Ali, G. Urbinati, M. Raouane and L. Massaad-Massade, *Expert Rev. Clin. Pharmacol.*, 2012, **5**, 403–412.
4 A. de Fougerolles, H. P. Vornlocher, J. Maraganore and J. Lieberman, *Nat. Rev. Drug Discovery*, 2007, **6**, 443–453.
5 Y. Li, H. Bai, H. Wang, Y. Shen, G. Tang and Y. Ping, *Nanoscale*, 2017, **10**, 203–214.
6 C. K. Chen, W. C. Law, R. Aalinkeel, Y. Yu, B. Nair, J. Wu, S. Mahajan, J. L. Reynolds, Y. Li, C. K. Lai, E. S. Tzanakakis, S. A. Schwartz, P. N. Prasad and C. Cheng, *Nanoscale*, 2014, **6**, 1567–1572.
7 S. Bhunia, V. Radha and A. Chaudhuri, *Nanoscale*, 2017, **9**, 1201–1212.
8 N. K. Ryoo, J. Lee, H. Lee, H. K. Hong, H. Kim, J. B. Lee, S. J. Woo, K. H. Park and H. Kim, *Nanoscale*, 2017, **9**, 15461–15469.
9 A. Daka and D. Peer, *Adv. Drug Delivery Rev.*, 2012, **64**, 1508–1521.
10 S. Quasthoff and H. P. Hartung, *J. Neurol.*, 2002, **249**, 9–17.
11 T. A. Ahles, A. J. Saykin, C. T. Furstenberg, B. Cole, L. A. Mott, K. Skalla, M. B. Whedon, S. Bivens, T. Mitchell, E. R. Greenberg and P. M. Silberfarb, *J. Clin. Oncol.*, 2002, **20**, 485–493.
12 D. H. Kim and J. J. Rossi, *Nat. Rev. Genet.*, 2007, **8**, 173–184.
13 B. Ozpolat, A. K. Sood and G. Lopez-Berestein, *Adv. Drug Delivery Rev.*, 2014, **66**, 110–116.
14 J. C. Burnett, J. J. Rossi and K. Tiemann, *Biotechnol. J.*, 2011, **6**, 1130–1146.
15 S. Gao, H. Tian, Z. Xing, D. Zhang, Y. Guo, Z. Guo, X. Zhu and X. Chen, *J. Controlled Release*, 2016, **243**, 357–369.
16 R. Molinaro, J. Wolfram, C. Federico, F. Cilurzo, L. Di Marzio, C. A. Ventura, M. Carafa, C. Celia and M. Fresta, *Expert Opin. Drug Delivery*, 2013, **10**, 1653–1668.
17 J. Beloor, C. S. Choi, H. Y. Nam, M. Park, S. H. Kim, A. Jackson, K. Y. Lee, S. W. Kim, P. Kumar and S. K. Lee, *Biomaterials*, 2012, **33**, 1640–1650.
18 C. He, Y. Hu, L. Yin, C. Tang and C. Yin, *Biomaterials*, 2010, **31**, 3657–3666.

19 J. Liu, S. Iqbal, X. J. Du, Y. Yuan, X. Yang, H. J. Li and J. Wang, *Biomater. Sci.*, 2018, **6**, 350–355.

20 R. A. Petros and J. M. DeSimone, *Nat. Rev. Drug Discovery*, 2010, **9**, 615–627.

21 H. Hatakeyama, H. Akita and H. Harashima, *Adv. Drug Delivery Rev.*, 2011, **63**, 152–160.

22 H. Hatakeyama, H. Akita, E. Ito, Y. Hayashi, M. Oishi, Y. Nagasaki, R. Danev, K. Nagayama, N. Kaji, H. Kikuchi, Y. Baba and H. Harashima, *Biomaterials*, 2011, **32**, 4306–4316.

23 N. P. Gabrielson, H. Lu, L. Yin, K. H. Kim and J. Cheng, *Mol. Ther.*, 2012, **20**, 1599–1609.

24 L. Yin, Z. Song, K. H. Kim, N. Zheng, N. P. Gabrielson and J. Cheng, *Adv. Mater.*, 2013, **25**, 3063–3070.

25 L. Yin, Z. Song, K. H. Kim, N. Zheng, H. Tang, H. Lu, N. Gabrielson and J. Cheng, *Biomaterials*, 2013, **34**, 2340–2349.

26 L. Yin, Z. Song, Q. Qu, K. H. Kim, N. Zheng, C. Yao, I. Chaudhury, H. Tang, N. P. Gabrielson, F. M. Uckun and J. Cheng, *Angew. Chem., Int. Ed.*, 2013, **52**, 5757–5761.

27 L. Yin, H. Tang, K. H. Kim, N. Zheng, Z. Song, N. P. Gabrielson, H. Lu and J. Cheng, *Angew. Chem., Int. Ed.*, 2013, **52**, 9182–9186.

28 N. Zheng, L. Yin, Z. Song, L. Ma, H. Tang, N. P. Gabrielson, H. Lu and J. Cheng, *Biomaterials*, 2014, **35**, 1302–1314.

29 R. Gref, A. Domb, P. Quellec, T. Blunk, R. H. Muller, J. M. Verbavatz and R. Langer, *Adv. Drug Delivery Rev.*, 1995, **16**, 215–233.

30 M. Li, W. Song, Z. Tang, S. Lv, L. Lin, H. Sun, Q. Li, Y. Yang, H. Hong and X. Chen, *ACS Appl. Mater. Interfaces*, 2013, **5**, 1781–1792.

31 W. Song, M. Li, Z. Tang, Q. Li, Y. Yang, H. Liu, T. Duan, H. Hong and X. Chen, *Macromol. Biosci.*, 2012, **12**, 1514–1523.

32 T. Akagi, H. Kim and M. Akashi, *J. Biomater. Sci., Polym. Ed.*, 2010, **21**, 315–328.

33 K. Zhang, X. Zhu, F. Jia, E. Auyeung and C. A. Mirkin, *J. Am. Chem. Soc.*, 2013, **135**, 14102–14105.

34 L. Miao, C. M. Lin and L. Huang, *J. Controlled Release*, 2015, **219**, 192–204.

35 E. A. Vasievich and L. Huang, *Mol. Pharm.*, 2011, **8**, 635–641.

36 X. Guan, Z. Guo, T. Wang, L. Lin, J. Chen, H. Tian and X. Chen, *Biomacromolecules*, 2017, **18**, 1342–1349.

37 Z. Guo, J. Chen, L. Lin, X. Guan, P. Sun, M. Chen, H. Tian and X. Chen, *ACS Appl. Mater. Interfaces*, 2017, **9**, 15297–15306.

38 Y. Yu, C. K. Chen, W. C. Law, E. Weinheimer, S. Sengupta, P. N. Prasad and C. Cheng, *Biomacromolecules*, 2014, **15**, 524–532.

39 X. Chen, L. Liu and C. Jiang, *Acta Pharm. Sin. B*, 2016, **6**, 261–267.

40 M. Dimde, F. Neumann, F. Reisbeck, S. Ehrmann, J. L. Cuellar-Camacho, D. Steinhilber, N. Ma and R. Haag, *Biomater. Sci.*, 2017, **5**, 2328–2336.

41 X. He, J. Li, S. An and C. Jiang, *Ther. Delivery*, 2013, **4**, 1499–1510.

42 P. Xu, E. A. Van Kirk, Y. Zhan, W. J. Murdoch, M. Radosz and Y. Shen, *Angew. Chem., Int. Ed.*, 2007, **46**, 4999–5002.

43 B. R. Voldborg, L. Damstrup, M. Spang-Thomsen and H. S. Poulsen, *Ann. Oncol.*, 1997, **8**, 1197–1206.

44 J. Du, W. L. Lu, X. Ying, Y. Liu, P. Du, W. Tian, Y. Men, J. Guo, Y. Zhang, R. J. Li, J. Zhou, J. N. Lou, J. C. Wang, X. Zhang and Q. Zhang, *Mol. Pharm.*, 2009, **6**, 905–917.

45 X. Guan, Z. Guo, L. Lin, J. Chen, H. Tian and X. Chen, *Nano Lett.*, 2016, **16**, 6823–6831.

46 R. Zhang, Z. Song, L. Yin, N. Zheng, H. Tang, H. Lu, N. P. Gabrielson, Y. Lin, K. Kim and J. Cheng, *Wiley Interdiscip. Rev.: Nanomed. Nanobiotechnol.*, 2015, **7**, 98–110.

47 J. Bugno, H. J. Hsu, R. M. Pearson, H. Noh and S. Hong, *Mol. Pharm.*, 2016, **13**, 2155–2163.

48 T. Jiang, Z. Zhang, Y. Zhang, H. Lv, J. Zhou, C. Li, L. Hou and Q. Zhang, *Biomaterials*, 2012, **33**, 9246–9258.

49 S. Guo, L. Lv, Y. Shen, Z. Hu, Q. He and X. Chen, *Sci. Rep.*, 2016, **6**, 21459.

50 Y. Sakurai, T. Hada, S. Yamamoto, A. Kato, W. Mizumura and H. Harashima, *Mol. Ther.*, 2016, **24**, 2090–2099.